benzocyclobutene. In the less fortunate cases, as for instance for the ethylenebenzenium ion structure **3**, a "structural specimen" is not available and structural assignment rests only on the fragmentation pattern of specifically labeled precursors. While such conclusions from the structural analysis of gaseous $C_8H_9^+$ ions by CA techniques are undoubtedly consistent with the spectra reported, their more general significance, and especially their use in structural comparison between gaseous ion and their condensed-phase counterparts, is hardly consistent with the present results and appear questionable in the light of the following considerations. It is generally recognized[20] that even the most sophisticated mass spectrometric tools for structural discrimination, such as CA techniques, suffer from serious limitations, in particular from the relatively long delay ($\geq 10^{-5}$ s) between the generation of the ion in the source of the spectrometer and its structural assay. During such a long lapse of time, structural rearrangements may occur, whose course and extent depend on the initial structure of the ion and its energy content. These parameters can be dramatically different in the "unknown" ion under investigation and in the ion used as its "structural model", since necessarily they arise from different ionization processes and/or from different neutrals. It follows that the observed similarity of their CA spectra, no matter how close, is not sufficient for concluding that both species are structurally identical. An indirect support to this statement is provided by the reported coincidence of the CA spectrum of the unknown structure X of the $C_8H_9^+$ family with that of the *exo*-cyclopropanonorbornyl ion, which can hardly be recognized as the thermodynamically most stable structure where any initially formed excited $C_8H_9^+$ ions isomerize under long-lived ($\geq 10^{-5}$ s) conditions.[5e,f]

On the other hand, the radiolytic technique adopted in this study allows effective collisional quenching of all the ionic species involved and their rapid sampling (lifetime $\leq 10^{-8}$ s) by reactive collisions with suitable acceptors. Under these conditions, ion rearrangement before sampling is substantially reduced, and positive structural discrimination of the ionic species is allowed by the direct determination of the isomeric composition of their neutral derivatives. The approach reveals interesting analogies between gas-phase adjacent phenyl-group assistance to cationic nucleophilic substitutions and related processes occurring under solvolytic conditions as well as in non-nucleophilic solvent media. The same reaction model seems to be operative in both the liquid and the gaseous phase, dominated in the latter by the polarization of phenyl group by the incipient positive charge at the reaction site, which in passing to condensed phases is progressively replaced by specific solvent assistance to the substitution process.

Acknowledgment. Support of our work by the Ministero della Pubblica Istruzione and by the Consiglio Nazionale delle Ricerche is gratefully acknowledged. It is a pleasure to acknowledge helpful discussion on the subject of this paper with F. Cacace; thanks are also due to V. Muraglia for his technical assistance.

Registry No. 4-F, 458-87-7; **4-Cl**, 622-24-2; **4-Me**, 32327-68-7; **4-OH**, 60-12-8; D_3^+, 12595-96-9; CH_5^+, 15135-49-6; $C_2H_5^+$, 14936-94-8; $CH_3FCH_3^+$, 64710-12-9.

(20) Dimerski, P. P.; McLafferty, F. W. *J. Am. Chem. Soc.* **1976**, *98*, 6070.

Effects of Chemical Environment on Direct Recoil Ion Fractions

J. N. Chen and J. W. Rabalais*

Contribution from the Department of Chemistry, University of Houston, Houston, Texas 77004.
Received March 11, 1987

Abstract: A qualitative model for describing a specific type of secondary particle emission, i.e., atoms which are directly recoiled (DR) from a surface as a result of a single primary ion collision, is developed. The model is used to interpret ion fractions of DR atoms from surfaces with differing chemical environments. Time-of-flight spectra of recoiled atoms resulting from 5-keV Ar^+ ions impingent on surfaces of Mg, MgO, $Mg(OH)_2$, Si, SiO_2, LiF, C_6F_6, and graphite have been obtained. Measurements of DR neutrals plus ions and neutrals only are used to calculate positive and negative ion fractions $Y_{+,-}$. These ion yields are sensitive to the chemical environment of the DR atom in the surface as follows. Y_+(Mg) from MgO is 10 times higher than from Mg metal and the SiO_2 surface yields higher $Y_{+,-}$(Si) than the Si surface. $Y_{+,-}$(F) from ionic LiF are larger than those from covalent C_6F_6 and Y_+(O) yields from oxides are particularly sensitive to the presence of hydrogen, decreasing as hydrogen concentration increases. Classical trajectory calculations are used to describe DR trajectories. The model for electronic charge exchange partitions the trajectory into two segments: (1) the close atomic encounter of the collision complex where electron promotions occur in the quasidiatomic molecule; (2) the outgoing trajectory where Auger and resonant electronic transitions occur. Analytical expressions for $Y_{+,-}$ are developed in terms of the probabilities involved and applied to interpretation of the experimental data.

I. Introduction

The mechanism by which specific charge states (positive, neutral, or negative) of secondary particles are produced during ion bombardment of surfaces remains an unsolved problem that is basic to a complete understanding of secondary ion mass spectrometry (SIMS),[1-4] ion scattering spectrometry (ISS),[5-9] and the sputtering behavior of materials.[10,11] Most investigations of charge states of secondary particles are concerned with particles emanating from a cascade sputtering mechanism,[12-14] and, although this is the ejection mechanism of most general interest,

(1) Schwartz, S. A.; Helms, C. R. *Surf. Sci.* **1981**, *102*, 578.
(2) Williams, P. *Surf. Sci.* **1979**, *90*, 588.
(3) Day, R. J.; Unger, S. E.; Cooks, R. G. *Anal. Chem.* **1980**, *52*, 557A.
(4) Colton, R. J.; Murday, J. S.; Wyatt, J. R.; DeCorpo, J. J. *Surf. Sci.* **1979**, *84*, 235.
(5) Buck, T. M.; Wheatly, G. H.; Verhei, L. K. *Surf. Sci.* **1979**, *90*, 635.
(6) Rabalais, J. W.; Schultz, J. A.; Kumar, R.; Murray, P. T. *J. Chem. Phys.* **1983**, *78*, 5250.
(7) Boers, A. L. *Nucl. Instrum. Methods Phys. Res., Sect. B* **1984**, *4*, 98; **1984**, *2*, 353.
(8) MacDonald, R. J.; O'Connor, D. J. *Surf. Sci.* **1983**, *124*, 423.
(9) Schneider, P. J.; Eckstein, W.; Verbeek, H. *Nucl. Instrum. Methods Phys. Res* **1982**, *194*, 387.
(10) Wittmaack, K. *Phys. Rev. Lett.* **1979**, *43*, 872.
(11) Harrison, D. E., Jr. *Radiat. Eff.* **1983**, *70*, 1.
(12) Deline, V. R.; Katz, W.; Evans, C. A.; Williams, P. *Appl. Phys. Lett.* **1978**, *33*, 832.
(13) Sander, P.; Kaiser, V.; Jede, R.; Lipinsky, D.; Granschow, O.; Benninghoven, A. *J. Vac. Sci. Technol.* **1985**, *3*, 1946.
(14) Yu, M. ;Reuter, W. *J. Vac. Sci. Technol.* **1980**, *17*, 36.

0002-7863/88/1510-0046$01.50/0

it is also the most complicated. Complications arise from the poorly defined collision energies, velocities, and trajectories of the sputtered particles. In cascade sputtering, the energy of the primary ion is dissipated to target atoms through collision cascades, some of which are eventually directed toward the surface and ejected. Such sputtered atom energy distributions peak at low energies[15] (1–20 eV) and are broad, tailing out to ca. 200 eV. The ion fraction in such distributions is typically small and very sensitive to surface conditions and type of bombarding ion, changing by orders of magnitude as a result of small perturbations. Post-ionization techniques[16] are used to probe the large neutral component of such cascade sputtered distributions.

In order to study a simpler, better defined process which may provide some insight for the more complicated cascade sputtered distributions, our group has investigated chemical effects on ion/neutral ratios of directly recoiled (DR) atoms. *DR atoms are surface atoms that are directly recoiled*[17,18] *into a forward scattering angle as a result of a direct collision from an energetic primary ion.* Such atoms have relatively narrow high-energy distributions, and the collision energy, DR atom velocity, trajectory, and point of origin are well-defined. For primary energies (E_0) in the keV range, the binary elastic collision model[19] provides a good description of the collision dynamics and can be used to calculate the energies (E_r) of DR atoms as well as those of quasisingle and quasimultiple scattered primaries. Since the DR particles have high velocities, it is possible to detect neutrals directly[20] using a channel electron multiplier and time-of-flight (TOF) techniques.

We have recently developed a model[21,22] for describing electronic transitions occurring during scattering and recoiling of keV particles from surfaces. The model considers that ions impingent on a surface can undergo charge exchange into the ground and excited states along the incoming and outgoing trajectories as well as additional neutralization, excitation, and ionization during the close atomic encounter. DR atoms first experience the close atomic encounter during the collision which is followed by the outgoing trajectory. During the close encounter we consider that electron promotions can occur within molecular orbitals (MO) of the quasidiatomic molecule formed during collision according to the Fano–Lichten mechanism;[23–25] both target and projectile atom can change their electronic and/or charge states as a result. Along the outgoing trajectory we consider that Auger and resonant charge exchange transitions, as described by Hagstrum,[26,27] can alter the final charge state of DR atoms.

The final charge states are determined as *differential ion fractions* $Y_{+,-}$, *i.e., the ratio of the number of positive or negative ions to the total number of particles recoiled or scattered into a specific solid angle.* These are differential rather than total ion fractions, the latter referring to the average ion fraction over the entire range of emission angles. Scattered ion fractions have now been measured for several ion/surface combinations with values ranging from 0 to 70% for noble gas ions on metal surfaces[21] and typically >80% for alkali ions.[28] Ion fractions for DR species have only recently[22] been measured and studied as a function of E_r. It has been shown[29] that DR species can have high positive and negative ion yields and that these yields exhibit different behavior as a function of E_r. Y_+ exhibits a threshold behavior and increases with E_r, while Y_- exhibits a low-energy maximum and decreases with E_r. This behavior has been interpreted[29] in terms of the model described above.

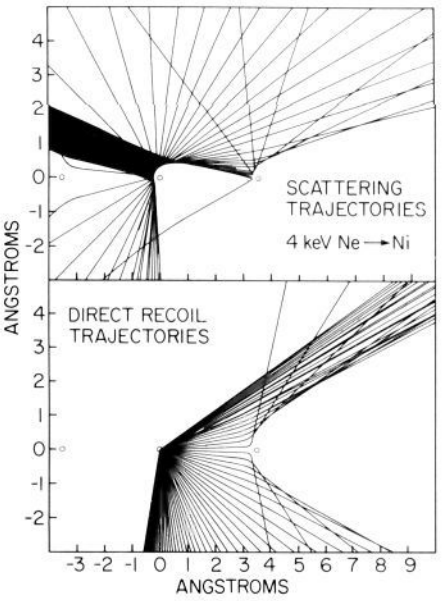

Figure 1. Classical trajectories of particles that are scattered and directly recoiled from a string of three target atoms. Note the formation of *shadow cones* behind the target atoms in scattering and a *blocking cone* behind the neighboring atom in direct recoiling.

The purpose of this paper is (i) to investigate the effects of chemical environment on ion yields of DR particles, (ii) to apply the above model for interpretation of the effects, and (iii) to use these results for gaining insight into the cascade sputtering problem. The paper is organized as follows. Section II considers classical dynamics, DR trajectories, and details of the model for DR ion yields. Experimental procedures for obtaining the DR spectra are presented in section III. The DR results presented in section IV include a description of spectral features in terms of the dynamics analysis and examples of DR ion fractions from various types of surfaces, including contrasting pairs such as metals/metal oxides, ionic/covalent, and semiconductors/insulators. The examples used include some new DR data as well as some previously published data. The discussion considers chemical effects on ion yields within the context of the model. The paper is concluded in section V with a consideration of the generality of the model and its ability to predict and interpret ion yields.

II. Dynamics of Direct Recoils

A. TOF–DR Spectrometry. In a DR experiment, a pulsed mass-selected ion beam with energy in the kilovolt range is directed onto a surface at a grazing angle of incidence resulting in pulses of scattered and recoiled particles. The energy or velocity distributions of both types of particles can be measured directly using either electrostatic analyzer (ESA) or time-of-flight (TOF) methods, respectively. The TOF method has the advantage of detecting both neutrals and ions simultaneously, hence the ability to determine ion yields without postionization techniques. The energy E_r of a target atom of mass M_2 recoiling from a primary ion of energy E_0 and mass M_1 is given from the binary collision model as

$$E_r = E_0[4A/(1 + A)^2] \cos^2 \theta \qquad (1)$$

where $A = M_2/M_1$ and θ is the recoil angle (angle between direction of incidence of the primary ion and recoiling target atom). From geometry considerations, DR is observed only at $\theta < 90°$.

(15) Vasile, M. J. *Surf. Sci.* **1982**, *115*, L141.
(16) Winograd, N.; Kobrin, P. H.; Schick, G. A.; Singh, J.; Baxter, J. P.; Garrison, B. J. *Surf. Sci.* **1986**, *176*, L817.
(17) Datz, S. D.; Snoek, C. *Phys. Rev. A* **1964**, *134*, 347.
(18) Buck, T. M.; Chen, Y. S.; Wheatley, G. H.; van der Weg, W. F. *Surf. Sci.* **1975**, *47*, 244.
(19) Smith, D. P. *J. Appl. Phys.* **1967**, *38*, 340.
(20) Chen, J. N.; Shi, M.; Tachi, S.; Rabalais, J. W. *Nucl. Instrum. Methods Phys. Res., Sect. B* **1986**, *16*, 91.
(21) Rabalais, J. W.; Chen, J. N.; Kumar, R.; Narayana, M. *J. Chem. Phys.* **1985**, *83*, 6489.
(22) Rabalais, J. W.; Chen, J. N. *J. Chem. Phys.* **1986**, *85*, 3615.
(23) Fano, U.; Lichten, W. *Phys. Rev. Lett.* **1965**, *14*, 627.
(24) Lichten, W. *J. Phys. Chem.* **1980**, *84*, 2102.
(25) Barat, M.; Lichten, W. *Phys. Rev. A* **1972**, *6*, 211.
(26) Hagstrum, H. D. *Phys. Rev.* **1954**, *96*, 336.
(27) Hagstrum, H. D. *Electron and Ion Spectroscopy of Solids*; Fiermans, L., Vennik, J., Dekeyser, W., Eds.; Plenum: New York, 1978.
(28) Boers, A. L. *Nucl. Instrum. Methods Phys. Res.* **1984**, *132*, 353.
(29) Chen, J. N.; Rabalais, J. W. *Nucl. Instrum. Methods Phys. Res., Sect. B* **1986**, *13*, 597.

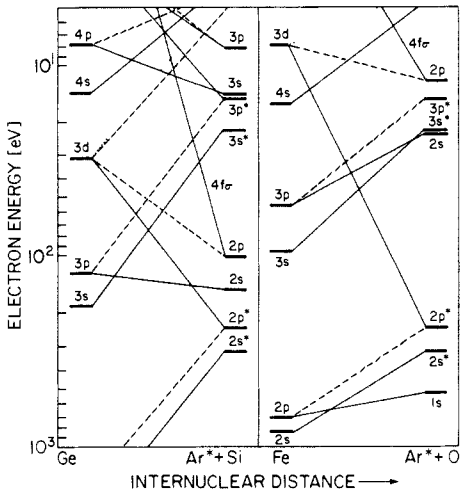

Figure 2. United atom (UA)–separated atom (SA) correlation diagram for electrons in a field of two differently charged nuclei. Diabatic MO's connect the levels of the infinitely separated atoms (right-hand side) with those of the united atom (left-hand side), maintaining the same value of the quantum number difference $(n - 1)$. The diagrams are specifically for Ar/Si and Ar/O collisions and experimental energy levels are used. MO's with $m = 0, 1, 2$ (σ, π, δ) are denoted by solid, dashed, and dotted lines, respectively.

Typical E_r values are greater than several hundred electron volts where they can be efficiently detected by a channel electron multiplier (CEM). The combination of low pulsed ion currents (<0.1 nA) and the multichannel analysis TOF technique allows collection of spectra with total ion doses $<10^{10}$ ions/cm^2, making the technique relatively nondestructive. Since both neutrals and ions are detected, quantitative analysis[30] of all elements, including hydrogen, on a surface can be obtained directly without complicated matrix effects. Because of the relatively short data acquisition times (several seconds), slow kinetics can be monitored[31] in real-time.

B. DR Trajectories. Examples of primary ion scattering and DR trajectories are shown in Figure 1 for the simple case of Ne^+ planar scattering along a string of three Ni target atoms. These classical trajectories have been obtained by integrating the equations of motion for all atoms involved. The calculation uses a model potential of the Biersack–Zeigler type[32] and assumes that the particles are elastically scattered; i.e., the recoil momentum is absorbed by the target atoms. Vibrational motions of the target atoms are neglected. Figure 1 shows the impinging Ne^+ incident from the left side at an angle of 20° to a line of Ni atoms with spacing 3.524 Å. The Ne^+ impact parameters are taken very close together in order to illustrate how a *shadow cone*, i.e., a region in which the impinging ions are excluded, is formed behind the target atom. The resulting scattered Ne^+ trajectories are shown going above the string as well as focused below the string (or into the crystal). The Ni DR trajectories resulting from this sequence of impact parameters are shown in the lower figure. The DR particles are primarily focused into a forward scattering direction as well as below the string (or into the crystal). Some of the DR trajectories at low exit angles are bent, or even deflected backwards, by the close proximity of the potential from the neighboring atom in the string. A *blocking cone* is formed around this neighboring atom. The DR trajectories show that recoiling particles spend a great deal of time near the surface where electronic charge transfer from neighboring atoms can occur.

C. Model for DR Ion Yields. For treatment of electronic charge exchange, we divide the direct recoil process into two parts, i.e., the close atomic encounter and the outgoing trajectory. These processes have been detailed in our previous papers;[21,22] hence they are covered only briefly here.

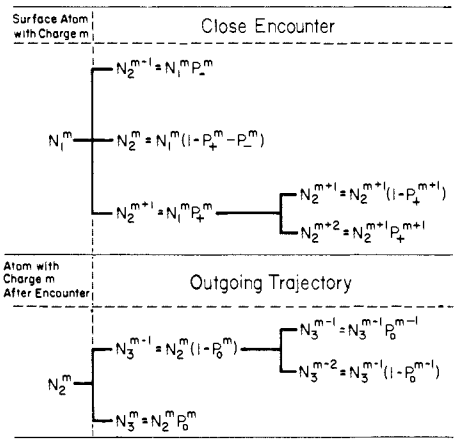

Figure 3. Derivation of the probability for consecutive charge exchange during the close encounter and outgoing trajectory of a DR sequence. The quantity $K(d\sigma/d\Omega)\Delta\Omega$ in eq 5 is set to unity for simplicity.

1. Close Atomic Encounter. In the close atomic encounter we define two processes, P_-^m and P_+^m, which are functions of the distance of closest approach s_0 for a given projectile–target combination. P_-^m is the probability that target atoms in charge state m will be reduced to charge state $(m - 1)$ and P_+^m is the probability that target atoms will lose one electron to produce charge state $(m + 1)$ as a result of the collision. The mechanism for P_-^m and P_+^m is according to the electron promotion model in the close encounter as described by united-separated atom diagrams, i.e., the Fano–Lichten (FL) mechanism.[23-25] Figure 2 shows an example of an FL diagram for Ar^+ collisions with O and Si. The probability expressions are derived from diagrams such as those of Figure 3 which outline the channels by which electrons are lost or gained by a DR atom. Here the subscripts 1, 2, and 3 denote respectively the undisturbed target atoms, the atom after the close encounter, and the atom infinitely far from the surface following the outgoing trajectory. Prior to the close encounter, we consider that the number of target atoms in charge state m is N_1^m. Following the encounter the charge states are described by N_2^n, where $n = -1$, 0, or 1; this limitation on n is used for simplification and because previous studies have shown that the fraction of multiply charged DR ions produced in this energy range is very low. The experimental data strongly support this assumption. As a result of this encounter, the target atom acquires energy according to eq 1 and proceeds along the trajectories of Figure 1 in either its original or an altered charge state.

2. Outgoing Trajectory. Electronic transitions along the outgoing trajectory are determined by the relative positions of the electronic energy levels of the solid and DR particle. These transitions can be divided into two categories, resonance and Auger transitions. Figure 4 shows valence and conduction bands for Mg metal and oxide along with the discrete first ionization potential of Mg, drawn inside the potential well of the departing atom. Letting N^m represent a DR particle of charge m and S represent a surface with n electrons in its valence band, a resonance transition can be represented as

$$N^m + ne_S^- \underset{2}{\overset{1}{\rightleftharpoons}} N^{m-1} + (n-1)e_S^- \qquad (2)$$

In such a *resonant surface-to-particle charge-transfer transition* $(S \rightarrow N)$, an electron tunnels from a filled level of the solid into a level containing a vacancy at the same energy in the particle. Transition 1 or $(S \rightarrow N)$ can occur only when the particle possesses a vacancy in the level E_i^v which is within the energy bounds $|E_F| < |E_i^v| < |E_B|$ or $|E_T| < |E_i^v| < |E_B|$. In a *resonant particle-to-surface charge-transfer transition* $(N \rightarrow S)$, an electron tunnels from a level of the particle into a vacancy in the solid conduction band at the same energy. Transition 2 or $(N \rightarrow S)$ can occur only when the particle possesses an occupied level E_i^0 which satisfies the condition $|E_c| < |E_i^0| < |E_F|$.

(30) Mintz, M. H.; Schultz, J. A.; Rabalais, J. W. *Surf. Sci.* **1984**, *146*, 457.
(31) Chen, J. N.; Kang, H.; Rabalais, J. W. *J. Am. Chem. Soc.*, submitted for publication.
(32) Ziegler, J. F.; Biersack, J. P.; Littmark, U. *The Stopping and Range of Ions in Solids*, Pergamon Press: New York, 1985.

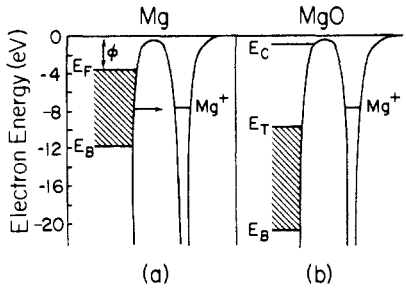

Figure 4. Electron energy diagrams representing a particle departing a surface as a result of a collision. The electronic band structures are for magnesium metal (a) and magnesium oxide (b), and the discrete ionization potential of Mg is shown in the potential well. The abscissa represents the distance from the surface to the departing particle, and the ordinate represents the energy of an electron in the solid or particle. The filled valence band is shown shaded. The most probable charge-transfer electronic transition that can occur between the particle and the surface while the departing particle is within ångstroms of the surface is indicated. This represents a resonance surface-to-particle (S → N) transition from the valence band to a vacant level, E_i^v, of the particle, e.g., resonance neutralization of a departing positive ion into an excited level or ground state of the neutral species. A resonance particle-to-surface (N → S) transition from an occupied level, E_i^0, of the particle into the conduction band can occur if the two levels are resonant. A two-electron Auger process in which a valence band electron tunnels into a particle vacancy at E_i^v and the energy gained is transferred to another valence band electron which can be excited into the conduction band or ejected into the continuum, e.g., Auger neutralization of a departing positive ion, can occur if $E_F < E_i^v$ for a metal and $E_i^v > 2E_T - E_C$ for an insulator.

A *two-electron or Auger surface-to-particle charge-transfer transition* (← S → N) involves the simultaneous transition of two electrons such as

$$N^m + ne_S^- \rightarrow N^{m-1} + (n-2)e_S^- + e^- \qquad (3)$$

In this process an electron from a filled valence band of the solid tunnels into the particle well and drops into a discrete vacant level; a second electron of the solid is excited into the conduction band or ejected into the continuum. An Auger transition can occur only when the particle possesses a vacancy in the level E_i^v which satisfies the conditions, for a metal $|E_F| < |E_i^v|$, and for an insulator $|E_T| < |E_i^v|$ and $|E_i^v| > |2E_T| - |E_C|$.

The electron exchange transition rate $R(s)$ along the outgoing trajectory is assumed to be a function of only the perpendicular distance s of the ion from the surface for a given particle–surface pair. Using a simple exponential rate function and defining the probability $P^m(s,v)$ that a particle with charge m and outgoing velocity v_0 perpendicular to the surface will reach $s = \infty$ in its original charge state, we obtain[21]

$$P_0^n(s,v_0) = \exp(A_0/av_0)[\exp(-as) - 1] \qquad (4)$$

Here A_0 (time^{-1}) is a preexponential constant and a (distance^{-1}) determines the particle–surface interaction range. At $s = \infty$ the charge states are described by N_3^n, where $n = m, m-1, \ldots, -1$. This limits electronic processes on the outgoing trajectory to electron pickup by the particle, i.e., charge reduction down to $n = -1$ rather than the endoergic process of electron loss by the particle, e.g., ionization.

3. Ion Fractions. Expressions for DR ion fractions are obtained by considering that a primary beam of N_0 ions impingent on a surface produces N^m DR particles according to

$$N^m = KN_0(d\sigma/d\Omega)\Delta\Omega nP^m \qquad (5)$$

where K is a spectrometer constant, $d\sigma/d\Omega$ is the differential DR cross section, $\Delta\Omega$ is the acceptance solid angle of the detector, n is the surface atom density, and P^m is the probability for atom N to be in charge state m at $s = \infty$ following a DR event. Limiting m to 1, 0, or −1, the probabilities for charge exchange P^{-1}, P^0, and P^+ can be traced as in Figure 3. The final DR ion fractions are determined as

$$Y_{+,-} = N^{+,-}/(N + N^+ + N^-) \qquad (6)$$

Table I. Expressions for $Y_{+,0,-}$ for Initial Neutral, Negative, and Positive Bonding Environments and the Limits of Y as $S_0 \rightarrow \infty$ and 0

	limits of $Y_{+,0,-}$	
	$s_0 \rightarrow \infty$, $v_0 \rightarrow 0$	$s_0 \rightarrow 0$, $v_0 \rightarrow \infty$
DR from Neutral Environment		
$Y_+ = P_+^0P_0^+$	0	P_+^0
$Y_0 = P_0^0(1 - P_+^0P_0^+)$	P_0^0	$1 - P_+^0$
$Y_- = 1 - P_0^0(1 - P_+^0P_0^+) - P_+^0P_0^+$	$1 - P_0^0$	0
DR from Negative Environment		
$Y_+ = P_+^-P_+^0P_0^+$	0	$P_+^-P_+^0$
$Y_0 = P_0^0P_+^-(1 - P_+^0P_0^+)$	0	$P_+^-(1 - P_+^0)$
$Y_- = 1 - P_0^0P_+^-(1 - P_+^0P_0^+) - P_+^-P_+^0P_0^+$	$Y_- = 1 - P_0^0P_+^-$	$1 - P_+^-$
DR from Positive Environment		
$Y_+ = P_0^+(1 - P_-^+)$	P_0^+	$1 - P_-^+$
$Y_0 = P_0^0[1 - P_0^+(1 - P_-^+)]$	$P_0^0(1 - P_0^+)$	P_-^+
$Y_- = 1 - P_0^+(1 - P_-^+) - P_0^0[1 - P_0^+(1 - P^+)]$	$1 - P_0^+ - P_0^0(1 - P_0^+)$	0

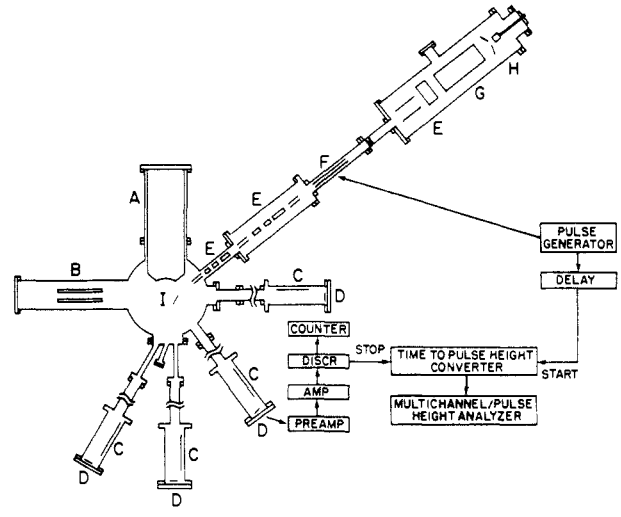

Figure 5. Schematic diagram of UHV chamber for TOF scattering and recoiling, X-ray and UV photoelectron spectroscopy (XPS and UPS), and mass spectrometry: (A) cylindrical mirror electron analyzer, (B) quadrupole mass spectrometer, (C) electrostatic deflector, (D) electron multiplier detector, (E) electrostatic lens, (F) pulse plates, (G) Wein filter, (H) Colutron ion source, and (I) sample. The UV and X-ray sources project out of the plane of this diagram and are not shown.

The sensitivity of $Y_{+,-}$ to the initial chemical environment of the surface can be obtained by using the scheme of Figure 3 to follow P^m of eq 5 for the various initial charge states m. The resulting $Y_{+,0,-}$ values are listed in Table I with the initial positive and negative charge states taken as +1 and −1. Although oxygen can exist in a −2 charge state, no O^{2-} is observed in DR; the transition probability $P_+(-2 \rightarrow -1)$ is assumed to be near unity in the close encounter. Consider the behavior of $Y_{+,0,-}$ of Table I in the limit of low and high kinetic energy. At low energy where s_0 is large, the inelastic processes in the close encounter become negligible; hence $P_+^m = P_-^m \rightarrow 0$ and the survival probabilities P_0^m control the yields of DR ions. In the high-energy limit, $v_0 \rightarrow \infty$, hence $P_0^m \rightarrow 1$, and the DR ion yield is dominated by the P_+^m and P_-^m inelastic processes of the close encounter. The resulting limits for the three charge states are listed in Table I.

III. Experimental Methods

The instrument for low-energy ion scattering and direct recoiling with TOF analysis and measurement of ion fractions is shown schematically in Figure 5. Operational details have been described previously.[21,22] Briefly, a Colutron ion source with range 0.1–10 keV equipped with Wien filter for mass selection, an off-axis aperture for elimination of neutrals, and an electronic chopper for primary ion pulse formation is used for the TOF experiments. TOF spectra are collected as a histogram of the distribution of particle flight times using a time-to-amplitude converter.

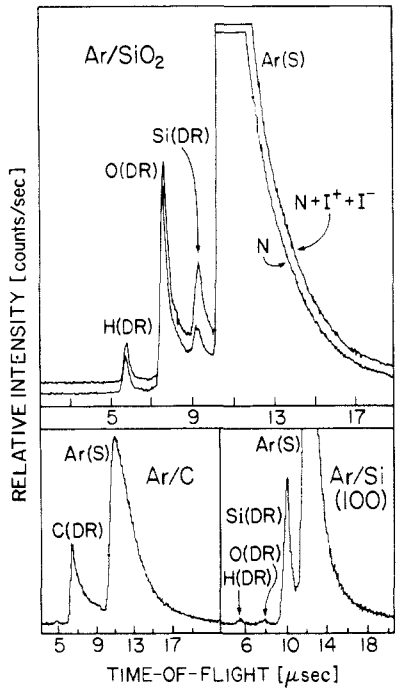

Figure 6. Time-of-flight spectra for Ar^+ bombardment of Si(100), SiO_2, and graphite at a 22° scattering and recoiling angle. Direct recoil of surface atoms is indicated by H(DR), O(DR), Si(DR), and C(DR), and Ar(S) represents scattered Ar; N + I = neutral + total ions and N = neutrals only.

Spectra of neutrals plus total ions (N + I) and neutrals only (N) were obtained by electrostatic deflection of the ions. Spectra of neutrals plus positive ions (N + I^+) and neutrals plus negative ions (N + I^-) were obtained by using a retarding grid in the flight path with either a negative or positive voltage, respectively, to retard unwanted ions. The operating conditions for these experiments are as follows: (1) primary beam: 5- or 6-keV Ar^+, 100-ns pulse width, 0.5-nA/cm^2 average current, 50-kHz pulse rate; (2) 22° scattering and recoil angle, 11° incident angle from the surface; (3) detector–channeltron electron multiplier with cone grounded; (4) ca. 3-kHz count rate for scattered and recoiled particles; (5) 2×10^{-10} torr base pressure. Investigations of channeltron detection efficiencies have shown[33,34] that preferential descrimination against neutrals for $E > 1$ keV is not significant.

The polycrystalline Mg and pyrolytic graphite samples were polished and cleaned by 3-keV Ar^+ bombardment using a separate sputtering gun in the same chamber. Oxidized and hydroxylated Mg were prepared by exposure to O_2 and H_2O as described elsewhere.[35] The Si(100) sample was cleaned by repeated heating to 1000 °C and Ar^+ bombardment. The SiO_2 was in the form of a 1000-Å thick film on a Si substrate and was cleaned by mild Ar^+ bombardment and annealing. Samples of LiF in the form of thin films on Rh foil were prepared[36] by in situ evaporation from research grade LiF using a tungsten boat. A hexafluorobenzene surface was obtained by chemisorption of 100 L of C_6F_6 on a Pt surface.

IV. Results and Discussion

A. TOF Scattering and Recoiling Spectra. Examples of TOF spectra for 5-keV Ar^+ scattering from Si, SiO_2, graphite, and LiF surfaces are shown in Figures 6 and 7. Spectra of ions (I) alone were obtained by subtracting the neutral (N) spectra from the (N + I) spectra. All of the spectra exhibit an intense peak at the calculated scattering (S) position. The lower intensity peaks at shorter TOF labeled (DR) result from recoiling surface atoms. It should be noted that even though the scattering angle is greater than the critical angle (17.5°) for single scattering of Ar from C, a sharp peak is still observed in the graphite spectrum; this peak is due to scattering by multiple collisions. The spectra show that the silicon and graphite samples could be cleaned to a condition where they were free of impurity recoils. The SiO_2 sample retained a small amount of hydrogen impurity, even after our best efforts at cleaning; it is likely that this hydrogen is distributed throughout the sample bulk. Spectra of the other samples have already been published in the literature: (Mg, MgO, $Mg(OH)_2$)[35] and (C_6F_6).[31]

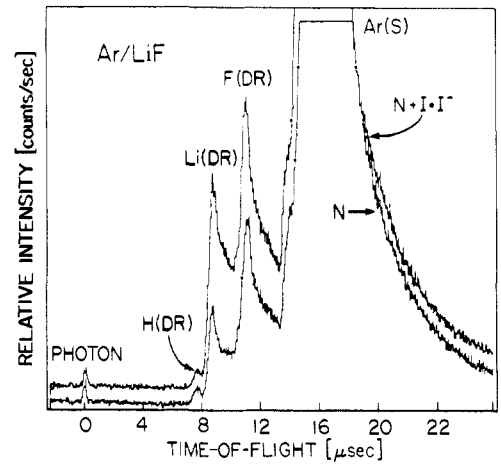

Figure 7. Time-of-flight spectra for Ar^+ bombardment of a LiF surface at a 22° scattering and recoiling angle. Direct recoil of surface atoms is indicated by Li(DR) and F(DR), and Ar(S) represents scattered Ar; N + I = neutral + total ions, and N = neutrals only.

B. Ion Yields for Metal/Metal Oxide Pairs. Consider the prediction of the model for the metal/metal oxide case using the expressions from Table I for Y_+ of a neutral species to describe Mg metal and a positive species to describe MgO. During the close Ar–Mg encounter, excitation energy is channeled dominantly into Mg through its 2p AO which correlates with the highly promoted 4fσ MO (Figure 2). Such a high degree of promotion[23-25] results in a signficant P_+^0 value for Mg metal. For MgO, we assume that Mg ions already exist in the surface and that some of them are neutralized according to P_-^+ (Table I). Thus, the result of the close encounter yields Mg^+ ion fractions of P_+^0 from Mg and $(1 - P_-^+)$ from MgO.

Along the outgoing trajectory, the (S → N) processes neutralize these emerging Mg^+ ions according to P_0^+. Figure 4 for Mg and MgO is typical for most metals and metal oxides. The work functions of most metals are normally several electron volts lower than the ionization potential of the corresponding ground-state metal atoms. There is usually an atomic level, E_i^v, which is isoenergetic with a valence band state of the solid, resulting in (S → N) processes for positive ions leaving a metal surface. Even for cases where $|E_i^v| > |E_B|$, (← S → N) processes can result in neutralization of emerging positive metal ions. Most negative metal ions have electron affinities <1 eV; such species can undergo (N → S) processes by transferring an electron from E_i^0 into the conduction band. Hence both positive and negative ions are efficiently neutralized from metal surfaces by the three processes described above. Note that the processes in the close encounter and along the outgoing trajectory for a metal are contradictory; i.e., even though P_+^0 efficiently produces ions, P_0^+ efficiently neutralizes them. For a metal oxide, the band gap (Figure 4) precludes neutralization of emerging positive ions for which the vacant level lies in the range E_C to E_T; hence the initial charge state of Mg^+ as it emerges is preserved at $s = \infty$ for this case.

The $Y_{+,-}$ values for Mg and MgO are listed in Table II. Y_+ for the MgO surface is 10 times higher than Y_+ for the Mg surface, and there are no observable Mg^- ions produced from either surface. This high Mg^+ yield from the oxide is typical for metal oxides and is a result of their original existence in the surface ($1 - P_-^+$) and the lack of neutralization processes P_0^+. The energy level diagram of Figure 4 along with the expressions of Table I qualitatively account for the yields of Mg^+ ions from metal/metal oxide pairs.

C. Ion Yields for Semiconductors/Insulators. The processes described above apply to semiconductors and insulators, with the

(33) Burrows, C. N.; Leiber, A. J.; Zaviantseff, V. T. *Rev. Sci. Instrum.* **1967**, *38*, 1477.
(34) Nersen, W. E., Jr.; Turner, W. C.; Cummins, W. F. *Rev. Sci. Instrum.* **1979**, *50*, 1227.
(35) Schultz, J. A.; Mintz, M. H.; Schuler, T. R.; Rabalais, J. W. *Surf. Sci.* **1984**, *146*, 438.
(36) Chen, J. N.; Rabalais, J. W. *Surf. Sci.* **1986**, *176*, L879.

Table II. Direct Recoil Ion Fractions, $Y_{+,-}$, for ϕ = 22° and 5-keV Ar^+ Bombardment of a Variety of Materials

surface	ion fractions (%)	
	$Y_+(Mg^+)$	
Mg	1.8	
MgO	18	
	$Y_+(Si^+)$	$Y_-(Si^-)$
Si	0.9	5.8
SiO_2	21.2	15.4
	$Y_+(F^+)$	$Y_-(F^-)$
C_6F_6/Pt	8.8	12.1
LiF	18.2	19.1
	$Y_+(C^+)$	$Y_-(C^-)$
C_6F_6/Pt	9.3	3.6
graphite	3.6	0.8
MgO and Mg(OH)		
[O/OH ratio]	$Y_+(O^+)$	$Y_-(O^-)$
17.4	9.8	23.7
8.9	6.1	26.9
6.0	5.5	27.8
1.1	1.0	34.1

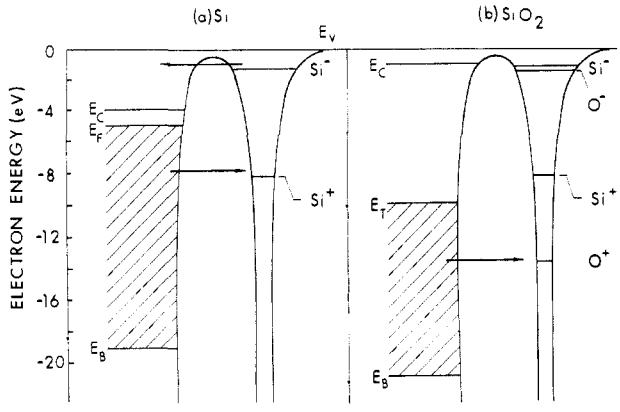

Figure 8. Electron energy diagrams representing DR particle emission from (a) silicon and (b) silicon dioxide.

major difference being the widths of the band gap, i.e., narrow for the former and broad for the latter. Consider Si and SiO_2 as examples of this pair; the $Y_{+,-}$ values are listed in Table II. Both are covalently bonded and we assume that the atoms are in a nearly neutral environment; hence we consider $Y_{+,-}$ of neutral species in Table I. The Si 2p AO is highly promoted through the 4fσ MO (Figure 2) which should result in a high P_+^0 value in the close encounter. Figure 8 shows that along the outgoing trajectory, for the Si case, Si^+ ions can be neutralized by (S → N) and (← S → N) transitions and Si^- ions can be neutralized by (N → S) transitions. Emerging neutrals cannot undergo (N → S) transitions to produce positive ions because the valence band of Si is filled. As a result, clean Si has a low Y^+ yield similar to metals. The fact that the Si^- yield is higher than the Si^+ yield from silicon indicates that the probability of negative ion production $(1 - P_0^0)$ along the trajectory is high relative to $(P_0^+P_+^0)$ of the positive ions.

For SiO_2 the large band gap makes it improbable for emerging Si^+ and Si^- to undergo charge exchange processes with the surface, resulting in enhanced $Y_{+,-}$ values. Note that $Y_-(SiO_2) > Y_-(Si)$; since there are no Si^- ions existing in the original bonding environment, these must be formed according to $(1 - P_0^0)$ along the outgoing trajectory and this probability is higher on the SiO_2 surface than on the Si surface.

D. Ion Yields for Ionic/Covalent Pairs. The $Y_{+,-}(F)$ yields from lithium fluoride and hexafluorobenzene are representative of ionic (negative F environment) and covalent (neutral F environment) systems, respectively. In the close encounter, the Ar/F energy level diagram is similar to that of Ar/O in Figure 2, where it is shown that the F 2p AO will correlate with the 4fσ MO resulting in promotion of F excited states. This implies that the processes P_+^- and P_+^0 of Table I are nonzero. The band structures of LiF and C_6F_6/Pt are shown in Figure 9; the surface of the latter is

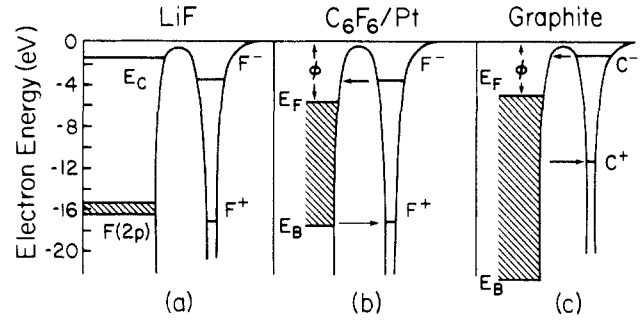

Figure 9. Electron energy diagram representing DR particle emission from (a) LiF, (b) C_6F_6, and (c) graphite.

represented by the Pt valence bands because the experiment used for comparison is C_6F_6 chemisorbed at low coverage (<1% monolayer) on a Pt surface. In the close encounter with F^- of LiF, F^+ is produced according to $(P_+^-P_+^0)$ and F^- survives the encounter according to $(1 - P_+^-)$. Along the outgoing trajectory, Figure 9 shows that (S → N) and (N → S) processes with the narrow valence bands are highly improbable. We surmise that ionic materials such as LiF represent a case where there is minimal exchange along the trajectory, and the observed $Y_{+,-}$ values are largely representative of electron promotion and exchange in the close encounter. Now consider the close encounter with F^0 of C_6F_6; F^+ is produced according to P_+^0. Along the outgoing trajectory, Figure 9 shows that F^+ can be neutralized by both (S → N) and (← S → N) and F^- is produced only by electron capture along the outgoing trajectory according to $(1 - P_0^0)$.

Table II shows that both $Y_+(F)$ and $Y_-(F)$ values from ionic LiF are larger than those from covalent C_6F_6 and that $Y_-(F) > Y_+(F)$ from both samples. The higher $Y_{+,-}$ values for the ionic surface are in agreement with the predictions of F^- already existing in that surface, F^+ being produced only in the encounter, and a low neutralization probability on ionic surfaces. The high $Y_-(F)/Y_+(F)$ ratio for both surfaces indicates that the survival probability of F^- along the trajectory is higher than that of F^+.

A closely related example is the $Y_{+,-}(C)$ values from graphite and C_6F_6/Pt. As the energy level diagram for graphite in Figure 9 shows, broad valence and conduction bands are available for charge exchange in both cases. The $Y_{+,-}(C)$ values listed in Table II are both higher for C_6F_6 than for graphite. Since the close encounter and the charge exchange along the trajectory are similar for these two systems, the different $Y_{+,-}$ values must reflect the original charge polarized environment of the C_6F_6 compound.

E. Ion Yields for Oxide/Hydroxide Pairs. The $Y_{+,-}(O)$ values for MgO and Mg(OH) are listed in Table II along with the O(DR)/H(DR) intensity ratio; the amount of hydroxide was controlled[35] by exposure of MgO to small doses of H_2. The ion yields are sensitive to the amount of hydroxide present, Y_- increasing by 31% and Y_+ decreasing by 90% from the pure oxide to the case O/OH = 1. Consider the case of the oxide. During the close encounter, s_0 = 0.28 Å[29] which is less than the sum of the radii of maximum radial charge density (0.62 Å) for the O and Ar L-atomic shells. This is close enough to produce highly excited and autoionizing states of oxygen, according to the promotion diagram of Figure 2, which can yield O^- and O^+ ions. Oxygen has a positive electron affinity of 1.54 eV; it is already in a negative state in the surface, O^- is more stable than O^+, and O^- has a higher probability of surviving charge exchange processes on the outgoing trajectory than O^+; all of these factors contribute to the high O^-/O^+ ratio from the oxide surface.

Next consider the hydroxide group. In a direct collision of Ar with a hydroxide moiety, most of the momentum will be transferred to the oxygen atom. The recoiling O and H atoms will have greatly different velocities, leading to dissociation of the OH group. It should be noted here that we have never observed molecules in DR spectra, indicating that the severity of the collision results in efficient dissociation. As the hydroxide moiety dissociates, we consider the dissociation products of OH^- and OH, the latter produced by charge exchange with Ar^+. As illustrated in Figure

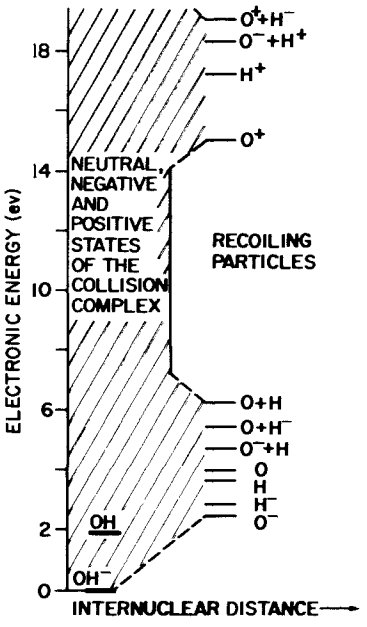

Figure 10. Energy level diagram illustrating the ground electronic states of OH^-, OH, and excited states of the Ar–O–H collision complex relative to states of the separated atoms, ions, and various combinations of atoms and ions.

10, the most stable products resulting from concerted dissociation of a negative hydroxide ion are $OH^- \rightarrow O^- + H$, whereas a neutral hydroxide group yields $OH \rightarrow O + H$ or $OH \rightarrow O^- + H^+$. During dissociation of a hydroxide moiety, the many potential energy curve crossings that result upon leaving the high density of states of the collision complex region favor production of the most stable products. Even for an unconcerted dissociation mechanism, O^- is also strongly favored over O^+ based on energetics as shown in Figure 10. The high sensitivity of $Y_+(O)$ to the presence of hydrogen strongly suggests that hydrogen is intimately involved in the dissociation mechanism. This large influence of hydrogen implies that there is concerted dissociation of OH^- and OH to yield the most stable products, i.e., $O^- + H$.

V. Conclusions

Direct recoils represent a specific type of secondary particle with well-defined trajectories which can be modeled by simple classical dynamics. The positive and negative *DR ion yields are sensitive to chemical effects*; i.e., the original chemical bonding environment in the surface has a strong influence on the charge of the outgoing particle. The qualitative model presented here is consistent with DR ion yields observed for a variety of surfaces, including metals, metal oxides, semiconductors, ionic/covalent compounds, and oxide/hydroxide pairs. The treatment identifies three important points in DR emission: (1) the initial charge state of the atom in the surface; (2) the close atomic encounter with the projectile in which ionization and neutralization probabilities are determined by electron promotion; and (3) the outgoing trajectory in which Auger and resonant charge-transfer transitions modify the final charge state of the DR particle. The model generates analytical expressions for the positive, neutral, and negative DR yields ($Y_{+,0,-}$) from differently charged bonding environments in terms of the probabilities for ionization, excitation, and neutralization in the close encounter along with the charge-exchange probability along the outgoing trajectory. The highest DR ion yields are obtained from ionic materials where the atoms are in initially charged states and the material has large band gaps and narrow valence bands with which charge exchange is improbable. The lowest DR ion yields are obtained from metals where the atoms are initially in neutral states and the valence and conduction bands are broad, facilitating charge exchange. The high sensitivity of the O^+ yield to the presence of hydrogen, i.e., decreasing as the hydrogen concentration increases, shows that dissociation of the OH group in the collision to yield the thermodynamically most stable species determines the final oxygen charge state. The model is proffered as a means of rationalizing and correlating the charge states of DR particles for different classes of materials and as a step toward elucidation of the more complex mechanism of charge states of cascade sputtered (SIMS) particles.

Acknowledgment. This material is based upon work supported by the National Science Foundation under Grant No. CHE-8513966 and by the Robert A. Welch Foundation under Grant No. E656. The classical trajectory program was written by Dr. P. Hochmann and M. Kilburn; we greatly appreciate their contributions.

Registry No. Ar^+, 14791-69-6; Mg, 7439-95-4; MgO, 1309-48-4; $Mg(OH)_2$, 1309-42-8; Si, 7440-21-3; SiO_2, 7631-86-9; LiF, 7789-24-4; C_6F_6, 392-56-3; H_2, 1333-74-0; Mg^+, 14581-92-1; Si^+, 14067-07-3; Si^-, 14337-02-1; F^+, 14701-13-4; F^-, 16984-48-8; C^+, 14067-05-1; C^-, 14337-00-9; O^+, 14581-93-2; O^-, 14337-01-0; graphite, 7782-42-5.